Adaptive Selection based Referring Image Segmentation

Anonymous Authors

ABSTRACT

Referring image segmentation (RIS) aims to segment a particular region based on a specific expression. Existing one-stage methods have explored various fusion strategies, yet they encounter two significant issues. Primarily, most methods rely on manually selected visual features from the visual encoder layers, lacking the flexibility to selectively focus on language-preferred visual features. Moreover, the direct fusion of word-level features into coarse aligned features disrupts the established vision-language alignment, resulting in suboptimal performance. In this paper, we introduce an innovative framework for RIS that seeks to overcome these challenges with adaptive alignment of vision and language features, termed the Adaptive Selection with Dual Alignment (ASDA). ASDA innovates in two aspects. Firstly, we design an Adaptive Feature Selection and Fusion (AFSF) module to dynamically select visual features focusing on different regions related to various descriptions. AFSF is equipped with scale-wise feature aggregator to provide hierarchically coarse features that preserve crucial low-level details and provide robust features for successor dual alignment. Secondly, a Word Guided Dual-Branch Aligner (WGDA) is leveraged to integrate coarse features with linguistic cues by word-guided attention, which effectively addresses the common issue of vision-language misalignment by ensuring that linguistic descriptors directly interact with masks prediction. This guides the model to focus on relevant image regions and make robust prediction. Extensive experimental results demonstrate that our ASDA framework surpasses state-of-the-art methods on RefCOCO, RefCOCO+ and G-Ref benchmark. The improvement not only underscores the superiority of ASDA in capturing fine-grained visual details but also its robustness and adaptability to diverse descriptions.

CCS CONCEPTS

• **Computing methodologies → Scene understanding**; **Image segmentation**.

KEYWORDS

referring image segmentation, vision-language alignment

1 INTRODUCTION

Referring image segmentation (RIS) [7, 15, 64] aims to predict a pixel-wise mask for objects referred to in a natural language expression. It yields great value for various applications such as language-based human-robot interaction [50] and image editing [2].

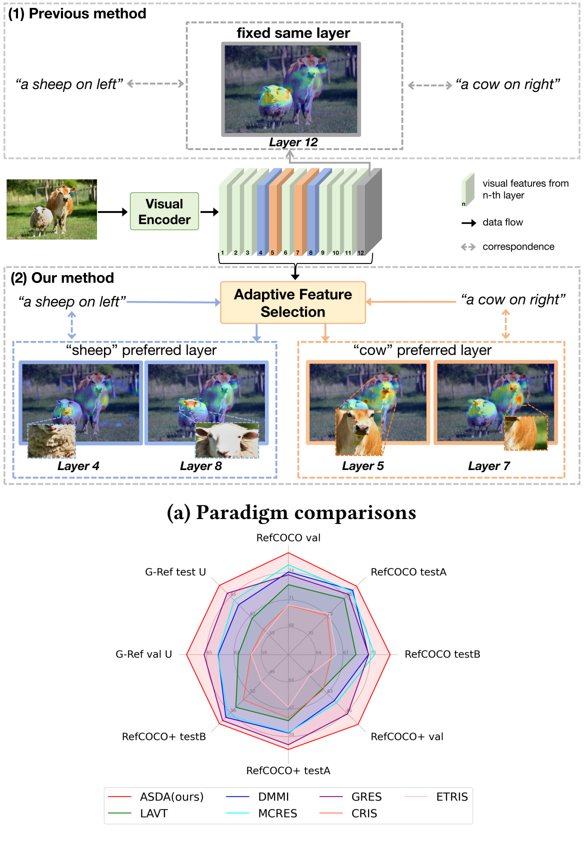

(a) Paradigm comparisons

(b) Qualitative comparisons

Figure 1: (a) Comparison of feature selection paradigm: The previous method utilizes features from fixed layers within the visual encoder regardless of the linguistic content, while our method adaptively selects the language-preferred features based on the specific language input. (b) Qualitative comparisons reveal that our ASDA framework outperforms previous state-of-the-art methods, achieving the best results across all splits on three datasets.

Unlike standard semantic segmentation [10, 12, 13], which categorizes image pixels based on a fixed set of labels, RIS needs to understand free-form language expression to locate the exact pixels of the referenced object. Hence, the primary challenge of this task involves achieving precise alignment between the relevant visual content and the descriptive text at the pixel level, which is crucial for accurately producing the necessary mask.

Existing methods [15, 29, 40] often leverage external knowledge to facilitate learning, typically relying on separate vision and language encoder, such as the Swin visual encoder [35] paired with the BERT language encoder [24], which inherently lacks multi-modal correspondence. Meanwhile, some studies [51, 54] have built on well-aligned model like CLIP [42], leveraging the advantages of vision-language pretraining. Regardless of the backbone choice,

ACM MM, 2024, Melbourne, Australia

ACM ISBN 978-x-xxxx-xxxx-x/YY/MM
https://doi.org/XXXXXXX.XXXXXXX

these methods commonly use manually determined visual features from the visual encoder layers, subsequently investing significant effort into feature fusion and alignment [4, 7, 18, 19, 23, 29, 34, 45, 51, 62]. Although these methods have promising performance, they encounter inherent challenges. Primarily, most methods rely on manually selected visual features from the visual encoder layers. As illustrated in Figure 1, when processing the same image with varying referring texts like "a sheep on the left" and "a cow on the right", these methods extract the same manually determined visual features. This manner lacks the flexibility to selectively focus on visual features that are more relevant to the specific language used. Moreover, the direct fusion between irrelevant visual features [7, 17, 51] with sentence-level language features introduces noise to subsequent word-level language features guided mask prediction, which results in disrupting the established vision-language alignments. As depicted in Figure 4, by visualizing the coarse features and the fine features, we observe that the fine features becomes disrupted after the interaction between the coarse features and word-level language features, focusing on regions unrelated to the textual description.

To this end, we propose an Adaptive Selection with Dual Alignment (ASDA) framework to enhance performance on RIS tasks, which mainly contains Adaptive Feature Selection and Fusion (AFSF) module and Word Guided Dual-Branch Aligner (WGDA) module. The Adaptive Feature Selection and Fusion (AFSF) module composes of Adaptive Feature Selection (AFS) module and Scale-Wise Feature Aggregator (SFA) module. Initially, AFS leverages sentence-level language features to select the most relevant features from the visual encoder layers. As shown in Figure 1, our AFS module can adaptively choose features that are more relevant to object described in the referring expression. Subsequently, SFA merges multi-scale visual features from AFS with sentence-level language features, effectively integrating semantics with the visual attributes of various layers. This provides hierarchically aggregated features that preserve crucial low-level details and offer robust features for successor dual alignment. Furthermore, we design two distinct branches in WGDA: the Coarse-to-Fine Segmentation Decoder (CFS) and the Word Guided Coefficient Generator (WCG), to more effectively interact word-level features with coarse features. The CFS utilizes robust features from AFSF module to generate candidate masks. Meanwhile, the WCG module employs a word-level language feature guided attention mechanism to generate the coefficients to combinate these masks. Unlike previous methods [22, 51, 59] that directly merge word-level language features into coarse features, our WGDA enables linguistic descriptors to directly interact with mask prediction without compromising the already aligned features, which helps get finely aligned visual feature.

In summary, the contribution of this work is fourfold:

- We propose an Adaptive Selection with Dual Alignment (ASDA) framework to enhance performance on RIS task.
- Our Adaptive Feature Selection and Fusion (AFSF) module dynamically selects the most relevant visual features based on language features, moving away from the conventional fixed-layer selection to a dynamic, text-responsive feature selection mechanism.
- Our Word Guided Dual-Branch Aligner (WGDA) module improves alignment and robustness of word-level features with visual features through a dual-branch structure, enhancing the interaction between linguistic descriptors and mask predictions.
- Our ASDA achieves state-of-the-art results on the RefCOCO, RefCOCO+, and RefCOCOg datasets.

2 RELATED WORK

Referring Image Segmentation (RIS) is designed to localize objects within images guided by natural language descriptions. The early approach [15] utilized a fusion technique combining linguistic and visual elements through concatenation. Subsequent efforts [4, 17, 21, 22, 29, 38] have harnessed sentence-level textual features from the descriptive phrases, whereas other studies [1, 9, 34, 40] have adopted word-level textual features for textual representation. Given that natural language intrinsically contains structured data [44, 57] that can be exploited to align with visual features, certain methodologies have decomposed expressions into various components [19, 52, 56, 58] or implemented a soft division approach using attention mechanisms [7, 10, 18, 45, 55, 62, 64].

Recent work has adopted more efficient structures for vision-language fusion. LAVT [59] utilizes the Swin Transformer [35] for visual tasks and incorporates modules for vision-language integration in the last four layers of the visual encoder. In contrast, ReSTR [25] and CRIS [51] start by separately encoding visual and linguistic inputs with a dual encoder, then merging these features either through a multi-modal transformer encoder or a cross-modal decoder. Inspired by the advancements in large language models [43, 48], new studies approach RIS as an auto-regressive generation task, introducing capabilities for logical reasoning [26, 63]. Recently, VPD [65] explores using semantic data from diffusion models [14, 46] for RIS applications, while ReLA [33] and DMMI [16] extend RIS capabilities to handle multiple targets.

Despite significant advances in RIS architecture, most methods face two main limitations. First, they depend on manually selected visual features from encoder layers, lacking flexibility to focus on language-preferred visual features for different objects. Additionally, most methods directly fuse word-level features with coarse visual features, leading to suboptimal performance. We introduce an innovative framework for RIS that seeks to overcome these challenges with adaptive selection and dual alignment of vision and language features.

Vision-Language Model (VLM) is a type of deep learning model designed to simultaneously interpret visual and textual information. These models can be categorized into two workflows: single-stream and dual-stream. Single-stream models, such as [3, 5, 6, 36], integrate vision and language embeddings using a unified self-attention encoder. In contrast, dual-stream models like CLIP [51], ALIGN [20], FILIP [61], and GLIP [28], employ separate encoders for each modality, aligning the outputs through a dot product. Other models such as ViLBERT [36] and LXMERT [47] utilize dual self-attention-based encoders to process within-modality interactions, while cross-attention mechanisms are used to handle interactions between modalities. As a milestone, CLIP [39] applies a contrastive learning approach across a vast dataset of image-text pairs, demonstrating significant transfer capabilities across over 30 classification datasets. Following this model, CRIS [51] uses a transformer decoder in conjunction with a CLIP model, adapting CLIP's text-to-image matching expertise to text-to-pixel applications. Given the outstanding performance of CLIP [39], we follow this well-aligned vision-language model to implement our framework.

3 METHOD

3.1 Overview

The framework of our proposed Adaptive Selection with Dual Alignment (ASDA) is illustrated in Figure 2. An image I and referring expressions T are fed to ViT-B based CLIP visual encoder (12 layers) and language encoder [39] respectively to extract layer-wise visual features $F_V^{(i)}$ and word-level, sentence-level language features $[f_T, f_E]$ (see Section 3.2). Next, Adaptive Feature Selection (AFS) module adaptively selects low-level visual features F_L from layers 4-6, middle-level visual features F_M from layers 7-9, high-level visual features F_H from highest layer of the Vision Encoder and generates multi-scale features $\tilde{F_L}$, $\tilde{F_M}$. Our Scale-Wise Feature Aggregator (SFA) then progressively fuses the global language features f_E with multi-scale visual features $\tilde{F_L}$, $\tilde{F_M}$, F_H, generating coarse aligned feature F_{coarse} (see Section 3.3). Finally, the Coarse-to-Fine Segmentation Decoder (CFS) processes F_{coarse} through Local Visual Attention and segmentation decoder to generate response masks M'. The Word-Guided Coefficient Generator (WCG) first combines the attention-enhanced feature F_A with word-level language feature f_T using Visual and Language Local Attention, generating fine feature F_{fine}. Following this, the Gated Coefficient Generation produces the coefficients f_{coef} corresponding to the masks M'. The final mask output $M \in \mathbb{R}^{H\times W}$ is then obtained by applying a weighted sum operation between the masks M' and the coefficients f_{coef} (see Section 3.4).

3.2 Features Extraction

Given an image I and referring expressions T, we extract layer-wise visual features $F_V^{(i)}$ and text features $[f_T, f_E]$ through ViT-B-based CLIP visual encoder and language encoder, respectively.

Image encoder. Following the design of vision transformer ViT, the image $I \in \mathbb{R}^{H_I \times W_I \times 3}$ is patched and projected to $I_P \in \mathbb{R}^{H\times W\times C}$, where $(H, W) = (H_I/P, W_I/P)$ and P indicates the resolution of each image patch. Then, I_P is fed into ViT [8] which employs N transformer layers. And the output of layer i is defined as $F_V^{(i)} \in \mathbb{R}^{H\times W\times C}$, $i = 0, \ldots, N$. The visual features of the final layer are recorded as the highest-level visual features F_H. Especially, there are 12 transformer layers in ViT-B. Each layer's visual features contain a learnable embedding which is called class token. The class token is recorded as the global visual features $f_C^{(i)} \in \mathbb{R}^C$.

Text encoder. For the given natural language referring expression, we extract word-level language feature $f_T \in \mathbb{R}^{N_T\times C}$ using a modified Transformer [49] architecture described in CLIP. Here, N_T represents the number of word-level language tokens. The expression sequence is enclosed with [SOS] and [EOS] tokens to indicate the start and end of sequences. The activations of the [EOS] token are considered as the sentence-level language feature $f_E \in \mathbb{R}^C$ for the entire natural language expression.

3.3 Adaptive Feature Selection and Fusion

As shown in Figure 2, the Adaptive Feature Selection and Fusion (AFSF) module consists of two main components: Adaptive Feature Selection (AFS) and Scale-Wise Feature Aggregator (SFA). Specifically, we design an adaptive selection network in ASF which is used to selectively identify the most relevant low-level visual feature F_L and mid-level visual feature F_M. Then it generates corresponding multi-scale features of low-level visual feature and mid-level visual feature, denoted as $\tilde{F_L}$ and $\tilde{F_M}$. Subsequently, the SFA module establishes the relationship between global language feature f_E and the highest-level local visual features F_H. Additionally, it fuses multi-scale features of low-level visual feature $\tilde{F_L}$ and mid-level visual feature $\tilde{F_M}$ to enhance the visual information of the target object, generating coarse feature F_{coarse}.

Adaptive Feature Selection (AFS). Based on our visual analysis in Figure 1, the visual features in different layers of the visual encoder can capture different local highlights related to various objects. When selecting the low-level visual feature F_L, the input includes global visual feature of the low-level visual feature candidate layers f_C^l, where $l \in \{4, 5, 6\}$, and the sentence-level language feature f_E. We first compute the cosine similarity between f_E and the class token f_C^l for each $l \in \{4, 5, 6\}$:

$$score^l = f_E \otimes \Phi_{\mathrm{T}}(f_C^l), \quad l \in \{4, 5, 6\} \tag{1}$$

where $score^l \in \mathbb{R}^C$, $\otimes$ means element-wise multiplication, Φ_{T} is a linear layer that maps the global visual feature f_C^l to the same dimension as $f_E \in \mathbb{R}^{1\times C}$. The score tokens $score^l$ serve a pivotal role in determining the alignment and relevance between textual descriptions and visual representations at different levels. They measure the similarity of visual features to textual descriptions, illustrating the relevance degree of correspondence. We then design an adaptive selection network based on $score^l$ to select the low-level visual feature:

$$\begin{gathered} score_L = \Phi_{\mathrm{as}}([score^4, socre^5, score^6]) \\ L = \Phi_{\mathrm{argmax}}(score_L) \\ F_L = F_V^{(L)} \end{gathered} \tag{2}$$

where $[,]$ denotes concatenation, Φ_{as} means adaptive selection network which is a combination of a Linear layer and softmax, $score_L \in \mathbb{R}^3$ represents the relevance scores of different feature layers processed through Φ_{as}, L is the index of the most relevant feature layer identified by Φ_{as} using Φ_{argmax}, and F_L is the feature of the ViT layer corresponding to the index L. Φ_{as} here serves a critical function in identifying the most appropriate feature layer index from the concated score tokens. There are many possible network architectures for Φ_{as}, but our experiments show that a simple combination of a linear layer and softmax yields the best results, as detailed in Table 5. The extraction of mid-level visual features F_M follows the similar way applied for low-level features, employing our proposed Adaptive Feature Selection network Φ_{as} to select the most related feature. This process is encapsulated as

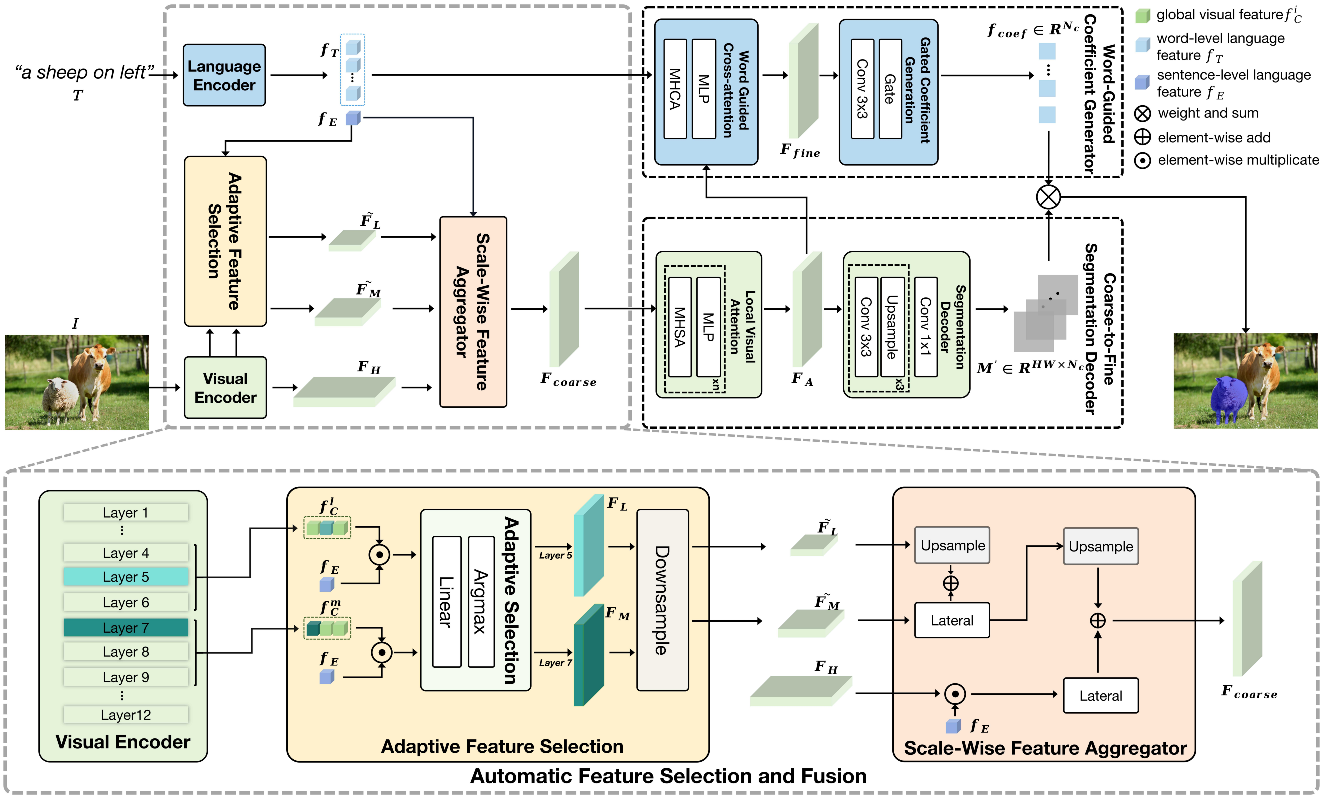

Figure 2: The overview of ASDA framework. It begins with extracting visual and language features from image I and referring text T. The Adaptive Feature Selection (AFS) module adaptively selects visual features F_L from Layers 4-6 and F_M from Layers 7-9 of the Visual Encoder and generates multi-scale features $\tilde{F_L}$, $\tilde{F_M}$. Our Scale-Wise Feature Aggregator (SFA) then progressively fuses the global language features f_E with high-level feature F_H together with multi-scale visual features $\tilde{F_L}$ and $\tilde{F_M}$, generating coarse feature F_{coarse}. Finally, the Coarse-to-Fine Segmentation Decoder (CFS) and Word-Guided Coefficient Generator (WCG) generate the final mask by using response masks M' and coefficients f_{coef}.

follows:

$$\begin{aligned} score^m &= f_E \cdot \Phi_{\mathrm{T}}(f_C^m), \quad m \in \{7, 8, 9\} \\ M &= \Phi_{\mathrm{argmax}}(\Phi_{\mathrm{as}}([score^7, score^8, score^9])) \\ F_M &= F_V^{(M)} \end{aligned} \tag{3}$$

Thus, we obtain the low-level visual features F_L, mid-level visual features F_M. Here we consider the output of the last layer of ViT-B as the highest-level feature F_H, which captures more global information in the image. All these three features have the same dimension $\mathbb{R}^{H \times W \times C}$. We then downsample the low-level and mid-level features. This process yields $\tilde{F_M} \in \mathbb{R}^{\frac{H}{2} \times \frac{W}{2} \times C}$ for mid-level feature and $\tilde{F_L} \in \mathbb{R}^{\frac{H}{4} \times \frac{W}{4} \times C}$ for low-level feature, facilitating a more detailed and hierarchical representation of visual information.

Scale-Wise Feature Aggregator (SFA). Inspired by the effectiveness of multi-scale features in the visual domain [11, 31, 67], we have adopted multi-scale features to enhance feature alignment. Unlike traditional tasks in the visual domain such as object detection [11, 31, 67] and segmentation [27, 66], maintaining the positional relationship between text and images when using multi-scale features in RIS settings presents a challenge. To solve this problem, we introduce the Scale-Wise Feature Aggregator (SFA) to preserve the spatial relationship between text and images from CLIP while leveraging multi-scale features. SFA initially combines global language feature f_E with top-layer visual features F_H, using element-wise multiplication:

$$f_G = f_H \odot f_E \tag{4}$$

where $f_H \in \mathbb{R}^C$ denotes the element of the top-layer visual features F_H and $f_G \in \mathbb{R}^C$ represents the single element of the global-to-local fused feature F_G. Subsequently, the global-to-local fused feature $F_G \in \mathbb{R}^{H \times W \times C}$ is integrated with the down-sampled low-level visual features $\tilde{F_L} \in \mathbb{R}^{\frac{H}{4} \times \frac{W}{4} \times C}$ and mid-level visual features $\tilde{F_M} \in \mathbb{R}^{\frac{H}{2} \times \frac{W}{2} \times C}$ through the following gradual process:

$$\begin{aligned} F_L' &= \Phi_{\mathrm{up}}(\tilde{F_L}) \\ F_M' &= \Phi_{\mathrm{lateral}}(\tilde{F_M}) + F_L' \\ F_{\mathrm{coarse}} &= \Phi_{\mathrm{agg}}(\Phi_{\mathrm{lateral}}(F_G) + \Phi_{\mathrm{up}}(F_M')) \end{aligned} \tag{5}$$

where the down-sampled low-level visual feature $\tilde{F_L}$ is initially 2x up-sampled by Φ_{up} to $F_L' \in \mathbb{R}^{\frac{H}{2} \times \frac{W}{2} \times 32}$ with channel reduction to 32. Concurrently, the down-sampled mid-level visual feature

$\tilde{F_M}$ is enhanced through Φ_{lateral} to achieve $F'_M \in \mathbb{R}^{H \times W \times 32}$, with channel reduction to 32. Φ_{lateral} here is a 1×1 Convolution-ReLU block. Based on our assumption that only basic information about the object location is needed, we boldly reduce the channel dimension to lower computational demands. The final aggregation step combines these enhanced features into $F_{\text{coarse}} \in \mathbb{R}^{HW \times C}$. This is achieved by employing a 3×3 convolution followed by a flattening operation via Φ_{agg}. This process is designed to restore the channel dimensions and then flatten the output for subsequent stages, effectively maintaining a balance between preserving details and ensuring computational efficiency in our approach to integrating multi-scale features.

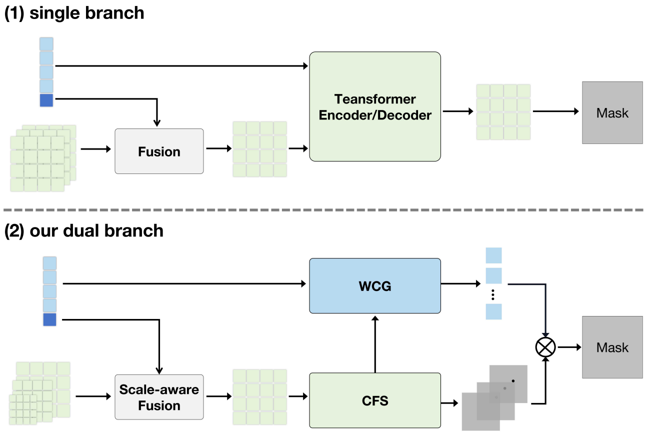

Figure 3: Illustration of single-branch cross-modal alignment in existing RIS methods and our dual alignment that enables linguistic descriptors to directly interact with mask prediction.

3.4 Word Guided Dual-Branch Aligner

As shown in Figure 4, the coarse feature map of CRIS [51] become disrupted after interaction with word-level language features, often focusing on regions unrelated to textual description. The previous single-branch alignment method [25, 51, 54] utilizes a Transformer Encoder or Decoder architecture to fuse coarse features with word-level language features, as demonstrated in Figure 3. To address this issue, we develop two distinct branches within the WGDA: Coarse-to-Fine Segmentation Decoder (CFS) and Word Guided Coefficient Generator (WCG), which more effectively align word-level features with coarse feature F_{coarse}. Specifically, the CFS branch utilizes Local Visual Attention and Segmentation Decoder to discern relationships among visual tokens and generate masks $M' \in \mathbb{R}^{HW \times N_c}$ focusing on different parts. The WCG branch comprises Visual and Language Local Attention and Gated Coefficient Generation, which find correspondences between word-level language features and local visual features to generate coefficients $f_{coef} \in \mathbb{R}^{N_c}$ for different response masks M'. And then we can get the final mask output $M \in \mathbb{R}^{H \times W}$ by applying a weighted sum operation between masks M' and coefficients f_{coef}. This design effectively preserves the alignment between global language and visual features while seamlessly incorporating word-level language features, avoiding the issues that come with single-branch.

Coarse-to-Fine Segmentation Decoder (CFS). Within the CFS branch, we first leverage the coarse aligned feature F_{coarse} as inputs to Local Visual Attention module, resulting in the attention-enhanced local visual features $F_A \in \mathbb{R}^{HW \times C}$. For Local Visual Attention module with n layers, the workflow of i-th layer is simplified as follows:

$$
\begin{aligned}
F_a^{(i-1)} &= \Phi_{\text{MHSA}}(\Phi_{\text{LN}}(F_{coarse})) + F_{coarse} \\
F_a^{(i)} &= \Phi_{\text{MLP}}(F_a^{(i-1)}) + F_a^{(i-1)}. \quad i = 1, 2, ..., n \\
F_A &= F_a^{(n)}
\end{aligned}
\tag{6}
$$

where $F_a^{(i-1)}$ represents the gradual refined visual features, Φ_{MHSA} indicates a multi-head self-attention layer and Φ_{LN} means Layer Normalization. After n layers of self-attention interaction, the Segmentation Decoder leverages the attention-enhanced visual features F_A to produce the response masks M', which is computed as follows:

$$
\begin{aligned}
F_A^{(i)} &= \Phi_{\text{conv}_{3\times3}}(\Phi_{\text{up}}(F_A^{i-1})), \quad i = 1, 2, 3 \\
F_A^{(4)} &= \Phi_{\text{conv}_{1\times1}}(F_A^{(3)}) \\
M &= \Phi_{\text{sigmoid}}(F_A^{(4)})
\end{aligned}
\tag{7}
$$

where Φ_{up} represents the upsampling operation, $\Phi_{\text{conv}_{3\times3}}$ denotes the convolution operation with a 3×3 kernel, $F_A^{(i)}$ denotes the feature after the i-th convolution and upsampling operation, and $\Phi_{\text{conv}_{1\times1}}$ indicates the final convolution operation with a 1×1 kernel. After the last convolution, the Φ_{sigmoid} function is applied to $F_A^{(4)}$ and then produce the response masks $M' \in \mathbb{R}^{HW \times N_c}$. Note that the hyperparameter n and N_c is discussed in the Table 3 and 4 in ablation study.

Word-Guided Coefficient Generator (WCG). Within WCG branch, we integrate the refined visual features F_A and the word-level language features f_T through the Visual and Language Local Attention module. The multi-head cross-attention layer is adopted to propagate fine-grained semantic information into the evolved visual features. The calculation is as follows:

$$
\begin{aligned}
F'_K &= \Phi_{\text{MHCA}}(\Phi_{\text{LN}}(F_A, f_T)) + F_A \\
F_{fine} &= \Phi_{\text{MLP}}(F'_K) + F'_K
\end{aligned}
\tag{8}
$$

where Φ_{MHCA} denotes the multi-head cross-attention layer, and F'_K is the intermediate features. The evolved multi-modal fine feature $F_{fine} \in \mathbb{R}^{HW \times C}$ which captures the relationship between word-level language features and local visual features is utilized for generating the coefficient f_{coef} through Gated Coefficient Generation module. The calculation is as follows:

$$
f_{coef} = \Phi_{\text{coef}}(F_{fine}) \tag{9}
$$

where Φ_{coef} comprises two stacked 3×3 convolution layers and one 1×1 convolution layer, followed by the Tanh activation function. The WCG branch effectively captures the essence of visual-textual interplay, producing normalized coefficients $f_{coef} \in \mathbb{R}^{N_c}$. Coefficients f_{coef} are then used to guide the segmentation output, ensuring a coherent integration of cross-modal insights.

Table 1: Comparisons with the state-of-the-art approaches on three benchmarks. We report the results of our method with various visual backbones. U: The UMD partition. G: The Google partition. “-” represents that the result is not provided. IoU is utilized as the metric.

Method	Visual	Language	RefCOCO			RefCOCO+			G-Ref			Avg
			val	testA	testB	val	testA	testB	val(U)	test(U)	val(G)	
CGAN [37]	DarkNet-53	Bi-GRU	64.86	68.04	62.07	51.03	55.51	44.06	51.01	51.69	46.54	54.98
LTS [22]	DarkNet-53	Bi-GRU	65.43	67.76	63.08	54.21	58.32	48.02	54.40	54.25	-	58.18
ReSTR [25]	ViT-B-16	GloVe	67.22	69.30	64.45	55.78	60.44	48.27	54.48	-	-	59.99
LAVT [59]	Swin-B	BERT	72.73	75.82	68.79	62.14	68.38	55.10	61.24	62.09	60.50	65.20
VLT [7]	Swin-B	BERT	72.96	75.96	69.60	63.53	68.43	56.92	63.49	66.22	62.80	66.66
SLViT [41]	SegNeXt	BERT	74.02	76.91	70.62	64.07	69.28	56.14	62.75	63.57	60.94	66.48
SADLR [60]	Swin-B	BERT	74.24	76.25	70.06	64.28	69.09	55.19	63.60	63.56	61.16	66.38
DMMI [16]	Swin-B	BERT	74.13	77.13	70.16	63.98	69.73	57.03	63.46	64.19	61.98	66.87
MCRES [53]	Swin-B	BERT	74.92	76.98	70.84	64.32	69.68	56.64	63.51	64.9	61.63	67.05
ReLA [33]	Swin-B	BERT	73.82	76.48	70.18	66.04	71.02	57.65	65.00	65.97	62.7	67.65
CRIS [51]	CLIP-R101	CLIP	70.47	73.18	66.1	62.27	68.08	53.68	59.87	60.36	-	64.25
ETRIS [54]	CLIP-ViT-B	CLIP	70.51	73.51	66.63	60.10	66.89	50.17	59.82	59.91	57.88	62.82
ASDA	**CLIP-ViT-B**	**CLIP**	**75.06**	**77.14**	**71.36**	**66.84**	**71.13**	**57.83**	**65.73**	**66.45**	**63.55**	**68.34**

Finally, the segmentation mask M is obtained by weighting and summing the coefficients $f_{coef} \in \mathbb{R}^{N_c}$ and the response mask $M' \in \mathbb{R}^{HW \times N_c}$:

$$M = \Phi_{\text{reshape}}(f_{coef} \otimes M') \tag{10}$$

where $M \in \mathbb{R}^{H \times W}$ represents the final output mask, $\otimes$ denotes the element-wise multiplication, and Φ_{reshape} is a reshaping operation that transforms the multiplied result into the desired output dimensions. Rather than adopting the contrastive learning proposed in CRIS, we supervise mask prediction through a linear combination of focal loss [32] and dice loss [30].

4 EXPERIMENTS

4.1 Datasets

We conduct extensive experiments on three benchmark datasets. **RefCOCO** stands out in this research domain, comprises 19, 994 images and 142, 210 referring expressions linked to 50, 000 objects. The dataset is divided into 120, 624 training, 10, 834 validation, 5, 657 test A, and 5, 095 test B images. It is characterized by typically containing two or more objects per image, with referring expressions averaging 3.6 words in length. **RefCOCO+** introduces an elevated challenge by omitting expressions containing certain absolute-location words. It includes 19, 992 images, presenting 49, 856 objects through 141, 564 linguistic expressions. The dataset is distributed across 120, 624 training, 10, 758 validation, 5, 726 test A, and 4, 889 test B samples. **G-Ref** distinguishes itself by using Amazon Mechanical Turk to collect 104, 560 referring expressions that describe 54, 822 objects in 26, 711 images. This collection method ensures greater linguistic diversity in the expressions, which averages 8.4 words and frequently mention locations and appearances. G-Ref is available in two versions, curated by the University of Maryland (UMD) and Google. Both versions have been utilized in our experiment.

4.2 Implementation Details

Experimental Settings. We firstly use ViT-B as the visual encoder and Transformer as the language encoder. Both the visual and language encoders are initialized with CLIP. Input images are resized to 416 × 416. The number N_c of response masks M' and coefficients f_{coef} are set to 32. The parameter n of Local Visual Attention module layers in CFS module is set to 2. The maximum length for the input natural language expression is set to 17 for RefCOCO and RefCOCO+, and 22 for G-Ref, including the [SOS] and [EOS] tokens. We use the Adam optimizer to train the network for 30 epochs with an initial learning rate of 5×10^{-5}, and we decay the learning rate in the 18^{th}, 25^{th} epochs with a decay rate of 0.1. We train the model with a batch size of 28 on 2 RTX 3090 GPUs.

Metrics. Following previous works, we adopt two metrics to verify the effectiveness: overall Intersection over Union (IoU) and Precision@X. IoU calculates the ratio of intersection to union regions between the predicted segmentation mask and the ground truth. Precision@X measures the percentage of test images that achieve an IoU score exceeding the threshold X, with X values of 0.5, 0.7, and 0.9.

4.3 Comparison with State-of-the-Art Methods

We evaluate our ASDA against state-of-the-art methods that utilize various visual and language backbones. Table 1 shows performance comparisons on three common splits of RefCOCO, RefCOCO+ and G-Ref. Compared to the recently SOTA ReLA [33] which uses Swin-B visual backbone [35] and BERT language backbone [24], our ASDA improves IoU by 1.24%, 0.66% and 1.18% on val, testA and testB splits of RefCOCO, respectively. On RefCOCO+, ASDA shows improvements of 0.80%, 0.11%, and 0.18% respectively for val, testA, and testB splits. Furthermore, on G-Ref dataset, improvements are 0.73% for val (U), 0.48% for test (U), and 0.85% for val (G) splits. This demonstrates that our ASDA not only achieves a better understanding of the location and appearance information in RefCOCO but also adapts to the various forms of expressions in RefCOCO+ and G-Ref. Besides, the following two comparisons show the effectiveness of our ASDA from different perspectives: (1) CRIS [51] is the first method which uses CLIP-R101 in RIS task. Compared to CRIS, our ASDA demonstrates significant performance improvements, with average gains of 4.6%, 3.92%, and 5.13% on RefCOCO, RefCOCO+, and G-Ref datasets, respectively. This demonstrates

Table 2: Ablation study on the validation set of RefCOCO. AFS: Automatic Feature Selection. SFA: Multi-scale Feature Aggregator. CFS: Coarse-to-Fine Segmentation Decoder. WGC: Word-Level Guided Cross-Attention.

	Method	val				test A				test B			
		P@0.5	P@0.7	P@0.9	IoU	P@0.5	P@0.7	P@0.9	IoU	P@0.5	P@0.7	P@0.9	IoU
(a)	baseline	76.98	62.80	14.92	66.70	81.40	69.08	15.53	70.02	70.10	53.89	17.21	62.43
(b)	(a)+manual assign	78.86	66.43	21.26	69.38	83.71	73.28	21.97	72.87	73.30	58.82	22.72	65.88
(c)	(a)+AFS	82.32	71.77	23.95	71.78	86.3	77.35	24.02	74.79	75.89	63.49	25.84	67.58
(d)	(a)+AFS+SFA	82.37	72.34	27.09	72.39	86.30	77.44	27.68	75.25	76.52	63.47	27.36	67.97
(e)	(d)+single-branch	85.97	76.76	28.72	74.65	88.45	81.36	28.76	76.54	79.50	68.45	29.55	70.62
(f)	**(d)+dual-branch(full)**	**86.37**	**77.74**	**29.80**	**75.06**	**89.28**	**82.23**	**29.96**	**77.14**	**80.76**	**69.61**	**30.14**	**71.36**

that our ASDA, equipped with the CLIP-ViT-B visual backbone, more effectively harnesses the spatial awareness capabilities of the ViT. (2) Compared to ETRIS [54] which uses CLIP ViT-B backbone, ASDA significantly surpasses them by 4.3%, 6.21% and 6.04% in terms of average IoU on RefCOCO, RefCOCO+ and G-Ref datasets respectively. This highlights ASDA's more effective use of CLIP's aligned vision-language features.

4.4 Ablation Study

To verify the effectiveness of our proposed components, we conduct comprehensive ablation studies to investigate each component on the RefCOCO val, test A, test B dataset. The components studied include Adaptive Feature Selection (AFS), Scale-Wise Feature Aggregator (SFA), Coarse-to-Fine Segmentation Decoder (CFS), and Word-Guided Coefficient Generator (WCG). The main results of the ablation study are presented in Table 2. Additionally, we have conducted ablation studies on the number of layers n in the Local Visual Attention module, the number of channels N_C in $f_{coef} \in \mathbb{R}^{N_c}$ and $M' \in \mathbb{R}^{HW \times N_c}$ and the architecture of adaptive selection (AS) network, which are presented in Table 3, 4 and 5 respectively. We limit the training of experiments in Table 3, 4, 5 to only 10 epochs and present the result on val split of RefCOCO , which leads to some differences in results compared to those in Table 2.

Baseline and manual assignment. (a) The baseline method extracts the highest-level visual feature F_H from the last layer of the visual encoder and fuses it with the global textual feature f_E using element-wise multiplication. The fused feature is then processed by the segmentation decoder to produce the final mask. (b) We enhance the baseline by employing a manual assignment approach following CRIS [51], manually selecting features from Layer 6 and Layer 9 as the low-level feature F_L and middle-level feature F_M respectively. These features F_L, F_M and F_H are then fused using the typical concatenation and projection method [51], without the use of multi-scale transformations. This improves 2.68%, 2.85%, 3.45% IoU on RefCOCO val, test A, test B respectively over (a), which demonstrates the significance of utilizing features from intermediate layers which focus on local regions.

Effect of Adaptive Feature Selection (AFS). (c) We replace the manual assignment (in Table 2 row 2) with our proposed Adaptive Feature Selection (AFS) module (in Table 2 row 3), which dynamically selects visual features using the global language feature f_E. In our setting, AFS will produce muti-scale visual features, here we just use the same fusion and decoder module as in (b). The 2.4%, 1.92% and 1.7% improvement of IoU on three splits compared to (b) shows our AFS module can adaptively choose features that are more relevant to object described in the referring expression, thereby enhancing segmentation accuracy.

Table 3: Ablation study on the hyperparameter n of the layers in the Local Visual Attention module.

n	P@0.5	P@0.7	P@0.9	IoU
1	82.38	71.64	23.97	71.72
2	**83.68**	**73.89**	**24.94**	**72.57**
3	82.08	71.94	25.92	72.13
4	83	72.37	24.79	72.57

Table 4: Ablation study on the hyperparameter N_C which represents the number of channels in $f_{coef} \in \mathbb{R}^{N_c}$ and $M' \in \mathbb{R}^{HW \times N_c}$.

N_C	P@0.5	P@0.7	P@0.9	IoU
16	79.68	68.16	22.2	70.61
32	**83.68**	**73.89**	**24.94**	**72.57**
48	82.46	71.9	24.91	71.92
64	82.25	70.6	24.25	71.78

Table 5: Ablation study on the architecture of adaptive selection network (as)

as	P@0.5	P@0.7	P@0.9	IoU
MLP	81.87	71.25	23.76	71.59
Conv	82.67	72.16	24.88	72.05
Linear	**83.68**	**73.89**	**24.94**	**72.57**

Effect of Scale-Wise Feature Aggregator (SFA). (d) We further validate the necessity of the Scale-Wise Feature Aggregator (SFA) module (in Table 2 row 4). Incorporating (c) with the SFA module, the IoU improves by 0.61%, 0.46% and 0.39% on three splits. This highlights the importance of multi-scale visual features in accurately capturing detailed characteristics of objects described in text.

Effect of Word Guided Dual-Branch Aligner (WGDA). We compare our proposed Word Guided Dual-Branch Aligner (WGDA) with previously proposed single-branch approaches [7, 17, 51]. As shown in Figure 3, (d) a single-branch approach directly interacts F_{coarse} from the ASFA module with word-level language features f_T, while (f) our WGDA method uses dual-branch to let inguistic descriptors directly interact with masks predictions. The results indicate that our WGDA outperforms the previous single-branch method by 0.41%, 0.6%, and 0.74% on three respective splits (in Table 2 row 5, 6). This indicates that our proposed Word Guided Dual-Branch Aligner (WGDA) can not only progressively refine visual features, but also effectively employ word-level language

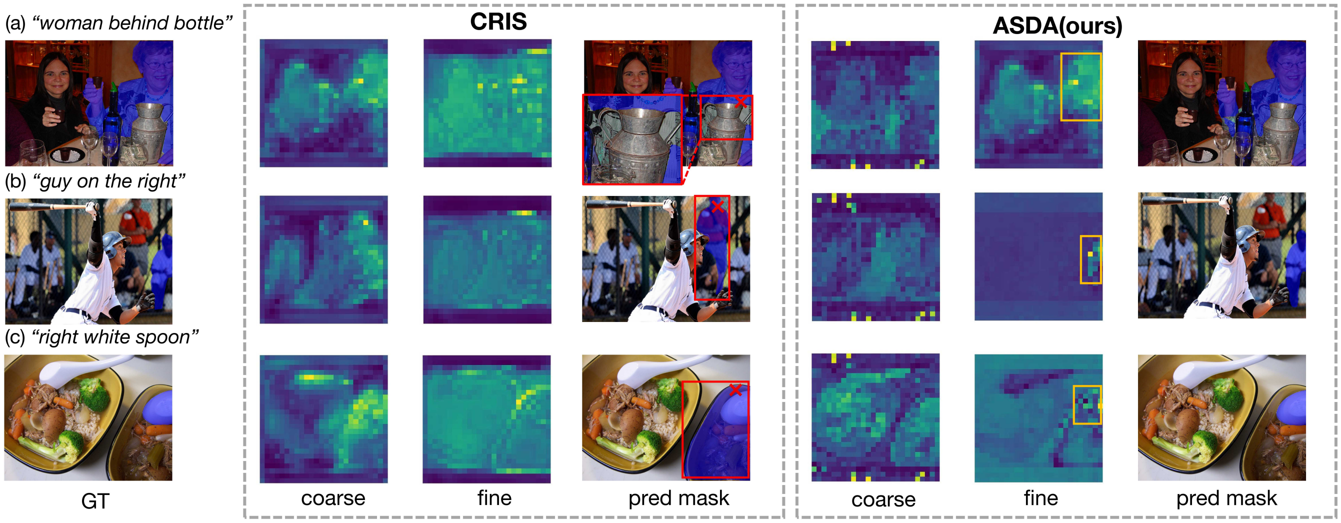

Figure 4: Visualization results of feature maps and final predicted mask in CRIS [51] and ASDA respectively. The coarse feature map represents the features without interaction with word-level language features, while the fine feature map results from the fusion and interaction between word-level features afterwards.

features f_T to guide coarse feature F_{coarse} to focus more on word-level language features, highlighting the importance of precise vision-language alignment.

Abalation about Adaptive selection (AS) network. In Table 5, we experiment different architectures within the adaptive selection (AS) network. In this experiment, we use our full model, only replacing the AS network layer. Specifically, we investigate three structures in the Adaptive Feature Selection (AFS) module to compute relevance scores: Linear, Convolution (Conv), and Multilayer Perceptron (MLP) layers. Each structure includes a softmax layer that transforms the scores into a probability distribution. Our findings indicate that the simple Linear layer configuration outperformed both the MLP and Conv layers, as evidenced by improvements in IoU of 0.98% and 0.52% over the val split of RefCOCO. This demonstrates that the Linear layer's simplicity and efficiency contribute to better generalization and performance.

Abalation about hyperparameter In Table 3, We conduct experiments to determine the most appropriate number of layers for Local Visual Attention within the Coarse-to-Fine Segmentation Decoder (CFS). We find that optimal performance is achieved when $n = 2$. In Equation 10, we obtain the final mask through weight and sum between response mask $M' \in \mathbb{R}^{HW \times N_c}$ and coefficients $f_{coef} \in \mathbb{R}^{N_c}$. As shown in Table 4, we conducted ablation studies on the hyperparameter N_C and found that the best performance is achieved when $N_C = 32$. As N_C exceeds the optimal value 32, performance declines due to overly complex model structure.

4.5 Qualitative Analysis

In Figure 4, we visualize the feature maps and the final predicted mask in CRIS [51] and our ASDA.

Comparison of Feature Maps. Comparing the coarse feature map, which is the fusion results between visual features from visual encoder and sentence-level language feature f_E, both CRIS and ASDA roughly capture the objects' semantic information. However, after interacting with word-level language features, the fine feature map in CRIS struggles to capture text-relevant features, leading to incorrect predictions. In contrast, the fine feature map from our ASDA, obtained after the Word Guided Cross-attention module in the Word-Guided Coefficient Generator (WCG) branch, can capture local visual detail. As shown by the yellow box in the Figure 4, our method's fine feature map can directly focus on visual features relevant to the text.

Comparison of Predicted Mask. The final predicted mask clearly demonstrates the superiority of our method. As indicated by the red box in the figure, for expression (a), CRIS fails to finely segment the part of the woman obscured by a bottle, whereas our method produces a detailed mask. In scenario (b), among multiple easily confusable objects, CRIS struggles to identify the correct person, while ASDA accurately locates the target, as already detected by fine feature map . For (c), CRIS incorrectly identifies the object, whereas ASDA produces an accurate and refined mask. More visualization results are provided in the Appendix.

5 CONCLUSION

In this paper, we introduce the Adaptive Selection with Dual Alignment (ASDA) framework for Referring Image Segmentation. Initially, our Adaptive Feature Selection and Fusion (AFSF) module dynamically selects visual features from vision encoder layers related to various descriptive texts. AFSF includes a scale-wise feature aggregator to provide hierarchically aggregated features that preserve crucial low-level details and robust features for dual alignment. Secondly, we utilize a Word Guided Dual-Branch Aligner (WGDA) that integrates visual features with linguistic cues through word-guided attention, effectively addressing vision-language misalignment by allowing linguistic descriptors to directly interact with mask predictions. This ensures focus on relevant image regions for robust predictions. Our extensive experiments show that ASDA outperforms state-of-the-art methods on the RefCOCO, RefCOCO+, and G-Ref benchmarks.

REFERENCES

[1] Ding-Jie Chen, Songhao Jia, Yi-Chen Lo, Hwann-Tzong Chen, and Tyng-Luh Liu. 2019. See-through-text grouping for referring image segmentation. In *Proceedings of the IEEE/CVF International Conference on Computer Vision*. 7454–7463.

[2] Jianbo Chen, Yelong Shen, Jianfeng Gao, Jingjing Liu, and Xiaodong Liu. 2018. Language-based image editing with recurrent attentive models. In *Proceedings of the IEEE conference on computer vision and pattern recognition*. 8721–8729.

[3] Yen-Chun Chen, Linjie Li, Licheng Yu, Ahmed El Kholy, Faisal Ahmed, Zhe Gan, Yu Cheng, and Jingjing Liu. 2019. Uniter: Learning universal image-text representations. (2019).

[4] Yi-Wen Chen, Yi-Hsuan Tsai, Tiantian Wang, Yen-Yu Lin, and Ming-Hsuan Yang. 2019. Referring expression object segmentation with caption-aware consistency. *arXiv preprint arXiv:1910.04748* (2019).

[5] Zhihong Chen, Yuhao Du, Jinpeng Hu, Yang Liu, Guanbin Li, Xiang Wan, and Tsung-Hui Chang. 2022. Multi-modal masked autoencoders for medical vision-and-language pre-training. In *International Conference on Medical Image Computing and Computer-Assisted Intervention*. Springer, 679–689.

[6] Zhihong Chen, Guanbin Li, and Xiang Wan. 2022. Align, reason and learn: Enhancing medical vision-and-language pre-training with knowledge. In *Proceedings of the 30th ACM International Conference on Multimedia*. 5152–5161.

[7] Henghui Ding, Chang Liu, Suchen Wang, and Xudong Jiang. 2021. Vision-language transformer and query generation for referring segmentation. In *Proceedings of the IEEE/CVF International Conference on Computer Vision*. 16321–16330.

[8] Alexey Dosovitskiy, Lucas Beyer, Alexander Kolesnikov, Dirk Weissenborn, Xiaohua Zhai, Thomas Unterthiner, Mostafa Dehghani, Matthias Minderer, Georg Heigold, Sylvain Gelly, et al. 2020. An image is worth 16x16 words: Transformers for image recognition at scale. *arXiv preprint arXiv:2010.11929* (2020).

[9] Guang Feng, Zhiwei Hu, Lihe Zhang, and Huchuan Lu. 2021. Encoder fusion network with co-attention embedding for referring image segmentation. In *Proceedings of the IEEE/CVF Conference on Computer Vision and Pattern Recognition*. 15506–15515.

[10] Jun Fu, Jing Liu, Haijie Tian, Yong Li, Yongjun Bao, Zhiwei Fang, and Hanqing Lu. 2019. Dual attention network for scene segmentation. In *Proceedings of the IEEE/CVF conference on computer vision and pattern recognition*. 3146–3154.

[11] Ross Girshick. 2015. Fast r-cnn. In *Proceedings of the IEEE international conference on computer vision*. 1440–1448.

[12] Junjun He, Zhongying Deng, Lei Zhou, Yali Wang, and Yu Qiao. 2019. Adaptive pyramid context network for semantic segmentation. In *Proceedings of the IEEE/CVF conference on computer vision and pattern recognition*. 7519–7528.

[13] Kaiming He, Georgia Gkioxari, Piotr Dollár, and Ross Girshick. 2017. Mask r-cnn. In *Proceedings of the IEEE international conference on computer vision*. 2961–2969.

[14] Jonathan Ho, Ajay Jain, and Pieter Abbeel. 2020. Denoising diffusion probabilistic models. *Advances in neural information processing systems* 33 (2020), 6840–6851.

[15] Ronghang Hu, Marcus Rohrbach, and Trevor Darrell. 2016. Segmentation from natural language expressions. In *Computer Vision–ECCV 2016: 14th European Conference, Amsterdam, The Netherlands, October 11–14, 2016, Proceedings, Part I 14*. Springer, 108–124.

[16] Yutao Hu, Qixiong Wang, Wenqi Shao, Enze Xie, Zhenguo Li, Jungong Han, and Ping Luo. 2023. Beyond one-to-one: Rethinking the referring image segmentation. In *Proceedings of the IEEE/CVF International Conference on Computer Vision*. 4067–4077.

[17] Zhiwei Hu, Guang Feng, Jiayu Sun, Lihe Zhang, and Huchuan Lu. 2020. Bi-directional relationship inferring network for referring image segmentation. In *Proceedings of the IEEE/CVF conference on computer vision and pattern recognition*. 4424–4433.

[18] Shaofei Huang, Tianrui Hui, Si Liu, Guanbin Li, Yunchao Wei, Jizhong Han, Luoqi Liu, and Bo Li. 2020. Referring image segmentation via cross-modal progressive comprehension. In *Proceedings of the IEEE/CVF conference on computer vision and pattern recognition*. 10488–10497.

[19] Tianrui Hui, Si Liu, Shaofei Huang, Guanbin Li, Sansi Yu, Faxi Zhang, and Jizhong Han. 2020. Linguistic structure guided context modeling for referring image segmentation. In *Computer Vision–ECCV 2020: 16th European Conference, Glasgow, UK, August 23–28, 2020, Proceedings, Part X 16*. Springer, 59–75.

[20] Chao Jia, Yinfei Yang, Ye Xia, Yi-Ting Chen, Zarana Parekh, Hieu Pham, Quoc Le, Yun-Hsuan Sung, Zhen Li, and Tom Duerig. 2021. Scaling up visual and vision-language representation learning with noisy text supervision. In *International conference on machine learning*. PMLR, 4904–4916.

[21] Yang Jiao, Zequn Jie, Weixin Luo, Jingjing Chen, Yu-Gang Jiang, Xiaolin Wei, and Lin Ma. 2021. Two-stage visual cues enhancement network for referring image segmentation. In *Proceedings of the 29th ACM international conference on multimedia*. 1331–1340.

[22] Ya Jing, Tao Kong, Wei Wang, Liang Wang, Lei Li, and Tieniu Tan. 2021. Locate then segment: A strong pipeline for referring image segmentation. In *Proceedings of the IEEE/CVF Conference on Computer Vision and Pattern Recognition*. 9858–9867.

[23] Sahar Kazemzadeh, Vicente Ordonez, Mark Matten, and Tamara Berg. 2014. Referitgame: Referring to objects in photographs of natural scenes. In *Proceedings of the 2014 conference on empirical methods in natural language processing (EMNLP)*. 787–798.

[24] Jacob Devlin Ming-Wei Chang Kenton and Lee Kristina Toutanova. 2019. BERT: Pre-training of Deep Bidirectional Transformers for Language Understanding. In *Proceedings of NAACL-HLT*. 4171–4186.

[25] Namyup Kim, Dongwon Kim, Cuiling Lan, Wenjun Zeng, and Suha Kwak. 2022. Restr: Convolution-free referring image segmentation using transformers. In *Proceedings of the IEEE/CVF Conference on Computer Vision and Pattern Recognition*. 18145–18154.

[26] Xin Lai, Zhuotao Tian, Yukang Chen, Yanwei Li, Yuhui Yuan, Shu Liu, and Jiaya Jia. 2023. Lisa: Reasoning segmentation via large language model. *arXiv preprint arXiv:2308.00692* (2023).

[27] Feng Li, Hao Zhang, Huaizhe Xu, Shilong Liu, Lei Zhang, Lionel M Ni, and Heung-Yeung Shum. 2023. Mask dino: Towards a unified transformer-based framework for object detection and segmentation. In *Proceedings of the IEEE/CVF Conference on Computer Vision and Pattern Recognition*. 3041–3050.

[28] Liunian Harold Li, Pengchuan Zhang, Haotian Zhang, Jianwei Yang, Chunyuan Li, Yiwu Zhong, Lijuan Wang, Lu Yuan, Lei Zhang, Jenq-Neng Hwang, et al. 2022. Grounded language-image pre-training. In *Proceedings of the IEEE/CVF Conference on Computer Vision and Pattern Recognition*. 10965–10975.

[29] Ruiyu Li, Kaican Li, Yi-Chun Kuo, Michelle Shu, Xiaojuan Qi, Xiaoyong Shen, and Jiaya Jia. 2018. Referring image segmentation via recurrent refinement networks. In *Proceedings of the IEEE Conference on Computer Vision and Pattern Recognition*. 5745–5753.

[30] Xiaoya Li, Xiaofei Sun, Yuxian Meng, Junjun Liang, Fei Wu, and Jiwei Li. 2019. Dice loss for data-imbalanced NLP tasks. *arXiv preprint arXiv:1911.02855* (2019).

[31] Yanghao Li, Hanzi Mao, Ross Girshick, and Kaiming He. 2022. Exploring plain vision transformer backbones for object detection. In *European Conference on Computer Vision*. Springer, 280–296.

[32] Tsung-Yi Lin, Priya Goyal, Ross Girshick, Kaiming He, and Piotr Dollár. 2017. Focal loss for dense object detection. In *Proceedings of the IEEE international conference on computer vision*. 2980–2988.

[33] Chang Liu, Henghui Ding, and Xudong Jiang. 2023. Gres: Generalized referring expression segmentation. In *Proceedings of the IEEE/CVF conference on computer vision and pattern recognition*. 23592–23601.

[34] Chenxi Liu, Zhe Lin, Xiaohui Shen, Jimei Yang, Xin Lu, and Alan Yuille. 2017. Recurrent multimodal interaction for referring image segmentation. In *Proceedings of the IEEE international conference on computer vision*. 1271–1280.

[35] Ze Liu, Yutong Lin, Yue Cao, Han Hu, Yixuan Wei, Zheng Zhang, Stephen Lin, and Baining Guo. 2021. Swin transformer: Hierarchical vision transformer using shifted windows. In *Proceedings of the IEEE/CVF international conference on computer vision*. 10012–10022.

[36] Jiasen Lu, Dhruv Batra, Devi Parikh, and Stefan Lee. 2019. Vilbert: Pretraining task-agnostic visiolinguistic representations for vision-and-language tasks. *Advances in neural information processing systems* 32 (2019).

[37] Gen Luo, Yiyi Zhou, Rongrong Ji, Xiaoshuai Sun, Jinsong Su, Chia-Wen Lin, and Qi Tian. 2020. Cascade grouped attention network for referring expression segmentation. In *Proceedings of the 28th ACM International Conference on Multimedia*. 1274–1282.

[38] Gen Luo, Yiyi Zhou, Xiaoshuai Sun, Liujuan Cao, Chenglin Wu, Cheng Deng, and Rongrong Ji. 2020. Multi-task collaborative network for joint referring expression comprehension and segmentation. In *Proceedings of the IEEE/CVF Conference on computer vision and pattern recognition*. 10034–10043.

[39] Huaishao Luo, Lei Ji, Ming Zhong, Yang Chen, Wen Lei, Nan Duan, and Tianrui Li. 2022. Clip4clip: An empirical study of clip for end to end video clip retrieval and captioning. *Neurocomputing* 508 (2022), 293–304.

[40] Edgar Margffoy-Tuay, Juan C Pérez, Emilio Botero, and Pablo Arbeláez. 2018. Dynamic multimodal instance segmentation guided by natural language queries. In *Proceedings of the European Conference on Computer Vision (ECCV)*. 630–645.

[41] Shuyi Ouyang, Hongyi Wang, Shiao Xie, Ziwei Niu, Ruofeng Tong, Yen-Wei Chen, and Lanfen Lin. 2023. Slvit: Scale-wise language-guided vision transformer for referring image segmentation. In *Proceedings of the Thirty-Second International Joint Conference on Artificial Intelligence, IJCAI-23*. 1294–1302.

[42] Alec Radford, Jong Wook Kim, Chris Hallacy, Aditya Ramesh, Gabriel Goh, Sandhini Agarwal, Girish Sastry, Amanda Askell, Pamela Mishkin, Jack Clark, et al. 2021. Learning transferable visual models from natural language supervision. In *International conference on machine learning*. PMLR, 8748–8763.

[43] Alec Radford, Karthik Narasimhan, Tim Salimans, Ilya Sutskever, et al. 2018. Improving language understanding by generative pre-training. (2018).

[44] Cheng Shi and Sibei Yang. 2022. Spatial and visual perspective-taking via view rotation and relation reasoning for embodied reference understanding. In *European Conference on Computer Vision*. Springer, 201–218.

[45] Hengcan Shi, Hongliang Li, Fanman Meng, and Qingbo Wu. 2018. Key-word-aware network for referring expression image segmentation. In *Proceedings of the European Conference on Computer Vision (ECCV)*. 38–54.

[46] Yang Song, Jascha Sohl-Dickstein, Diederik P Kingma, Abhishek Kumar, Stefano Ermon, and Ben Poole. 2020. Score-based generative modeling through stochastic differential equations. *arXiv preprint arXiv:2011.13456* (2020).

[47] Hao Tan and Mohit Bansal. 2019. Lxmert: Learning cross-modality encoder representations from transformers. *arXiv preprint arXiv:1908.07490* (2019).

[48] Hugo Touvron, Thibaut Lavril, Gautier Izacard, Xavier Martinet, Marie-Anne Lachaux, Timothée Lacroix, Baptiste Rozière, Naman Goyal, Eric Hambro, Faisal Azhar, et al. 2023. Llama: Open and efficient foundation language models. *arXiv preprint arXiv:2302.13971* (2023).

[49] Ashish Vaswani, Noam Shazeer, Niki Parmar, Jakob Uszkoreit, Llion Jones, Aidan N Gomez, Łukasz Kaiser, and Illia Polosukhin. 2017. Attention is all you need. *Advances in neural information processing systems* 30 (2017).

[50] Xin Wang, Qiuyuan Huang, Asli Celikyilmaz, Jianfeng Gao, Dinghan Shen, Yuan-Fang Wang, William Yang Wang, and Lei Zhang. 2019. Reinforced cross-modal matching and self-supervised imitation learning for vision-language navigation. In *Proceedings of the IEEE/CVF conference on computer vision and pattern recognition*. 6629–6638.

[51] Zhaoqing Wang, Yu Lu, Qiang Li, Xunqiang Tao, Yandong Guo, Mingming Gong, and Tongliang Liu. 2022. Cris: Clip-driven referring image segmentation. In *Proceedings of the IEEE/CVF conference on computer vision and pattern recognition*. 11686–11695.

[52] Chenyun Wu, Zhe Lin, Scott Cohen, Trung Bui, and Subhransu Maji. 2020. Phrasecut: Language-based image segmentation in the wild. In *Proceedings of the IEEE/CVF Conference on Computer Vision and Pattern Recognition*. 10216–10225.

[53] Li Xu, Mark He Huang, Xindi Shang, Zehuan Yuan, Ying Sun, and Jun Liu. 2023. Meta compositional referring expression segmentation. In *Proceedings of the IEEE/CVF Conference on Computer Vision and Pattern Recognition*. 19478–19487.

[54] Zunnan Xu, Zhihong Chen, Yong Zhang, Yibing Song, Xiang Wan, and Guanbin Li. 2023. Bridging vision and language encoders: Parameter-efficient tuning for referring image segmentation. In *Proceedings of the IEEE/CVF International Conference on Computer Vision*. 17503–17512.

[55] Sibei Yang, Guanbin Li, and Yizhou Yu. 2019. Dynamic graph attention for referring expression comprehension. In *Proceedings of the IEEE/CVF International Conference on Computer Vision*. 4644–4653.

[56] Sibei Yang, Guanbin Li, and Yizhou Yu. 2020. Graph-structured referring expression reasoning in the wild. In *Proceedings of the IEEE/CVF conference on computer vision and pattern recognition*. 9952–9961.

[57] Sibei Yang, Guanbin Li, and Yizhou Yu. 2020. Propagating over phrase relations for one-stage visual grounding. In *Computer Vision–ECCV 2020: 16th European Conference, Glasgow, UK, August 23–28, 2020, Proceedings, Part XIX 16*. Springer, 589–605.

[58] Sibei Yang, Meng Xia, Guanbin Li, Hong-Yu Zhou, and Yizhou Yu. 2021. Bottom-up shift and reasoning for referring image segmentation. In *Proceedings of the IEEE/CVF Conference on Computer Vision and Pattern Recognition*. 11266–11275.

[59] Zhao Yang, Jiaqi Wang, Yansong Tang, Kai Chen, Hengshuang Zhao, and Philip HS Torr. 2022. Lavt: Language-aware vision transformer for referring image segmentation. In *Proceedings of the IEEE/CVF Conference on Computer Vision and Pattern Recognition*. 18155–18165.

[60] Zhao Yang, Jiaqi Wang, Yansong Tang, Kai Chen, Hengshuang Zhao, and Philip HS Torr. 2023. Semantics-aware dynamic localization and refinement for referring image segmentation. In *Proceedings of the AAAI Conference on Artificial Intelligence*, Vol. 37. 3222–3230.

[61] Lewei Yao, Runhui Huang, Lu Hou, Guansong Lu, Minzhe Niu, Hang Xu, Xiaodan Liang, Zhenguo Li, Xin Jiang, and Chunjing Xu. 2021. Filip: Fine-grained interactive language-image pre-training. *arXiv preprint arXiv:2111.07783* (2021).

[62] Linwei Ye, Mrigank Rochan, Zhi Liu, and Yang Wang. 2019. Cross-modal self-attention network for referring image segmentation. In *Proceedings of the IEEE/CVF conference on computer vision and pattern recognition*. 10502–10511.

[63] Haoxuan You, Haotian Zhang, Zhe Gan, Xianzhi Du, Bowen Zhang, Zirui Wang, Liangliang Cao, Shih-Fu Chang, and Yinfei Yang. 2023. Ferret: Refer and ground anything anywhere at any granularity. *arXiv preprint arXiv:2310.07704* (2023).

[64] Licheng Yu, Zhe Lin, Xiaohui Shen, Jimei Yang, Xin Lu, Mohit Bansal, and Tamara L Berg. 2018. Mattnet: Modular attention network for referring expression comprehension. In *Proceedings of the IEEE conference on computer vision and pattern recognition*. 1307–1315.

[65] Wenliang Zhao, Yongming Rao, Zuyan Liu, Benlin Liu, Jie Zhou, and Jiwen Lu. 2023. Unleashing text-to-image diffusion models for visual perception. In *Proceedings of the IEEE/CVF International Conference on Computer Vision*. 5729–5739.

[66] Sixiao Zheng, Jiachen Lu, Hengshuang Zhao, Xiatian Zhu, Zekun Luo, Yabiao Wang, Yanwei Fu, Jianfeng Feng, Tao Xiang, Philip HS Torr, et al. 2021. Rethinking semantic segmentation from a sequence-to-sequence perspective with transformers. In *Proceedings of the IEEE/CVF conference on computer vision and pattern recognition*. 6881–6890.

[67] Xizhou Zhu, Weijie Su, Lewei Lu, Bin Li, Xiaogang Wang, and Jifeng Dai. 2020. Deformable detr: Deformable transformers for end-to-end object detection. *arXiv preprint arXiv:2010.04159* (2020).